Applied Catalysis B: Environmental 180 (2016) 301–311

Contents lists available at ScienceDirect

Applied Catalysis B: Environmental

journal homepage: www.elsevier.com/locate/apcatb

Bulk and γ-Al_2O_3-supported Ni_2P and MoP for hydrodeoxygenation of palmitic acid

Marco Peroni[a,1], Gabriella Mancino[b,1], Eszter Baráth[a], Oliver Y. Gutiérrez[a,*], Johannes A. Lercher[a,*]

[a] Technische Universität München, Department of Chemistry, Catalysis Research Center, Lichtenbergstraße 4, 85748 Garching, Germany
[b] Istituto di Ricerche sulla Combustione, Piazzale Tecchio 80, 80125 Naples, Italy

ARTICLE INFO

Article history:
Received 19 March 2015
Received in revised form 29 May 2015
Accepted 19 June 2015
Available online 24 June 2015

Keywords:
Hydrodeoxygenation
Ni_2P
MoP
Transition metal phosphides
Bio-oil

ABSTRACT

The use of a series of bulk and supported Ni_2P and MoP materials in the hydrodeoxygenation of palmitic acid, shows that their catalytic performance can be tuned by the presence of Al_2O_3 as a support. Al_2O_3 promotes acid-catalyzed pathways, and influences the phosphide functionality. A series of strategies can be followed to successfully decrease the phosphide particle size, i.e., the use of citric acid (applied to bulk Ni_2P), and the use of low reduction temperatures (applied to Ni_2P/Al_2O_3) during the preparation steps. The effects of synthesis parameters and the support on the properties of the phosphides were determined by, e.g., X-ray diffraction, transmission electron microscopy, BET analysis, CO adsorption and NH_3-TPD. Small particle size of phosphides does not necessarily lead to a large exposed surface of metal phosphide due to residual carbon or to agglomeration of phosphide particles. The specific activities (per gram of material) follow the trend MoP/Al_2O_3-TPR (high temperature synthesis) < Ni_2P-CA (citric acid in the synthesis) < Ni_2P/Al_2O_3-LT (low temperature synthesis) < Ni_2P/Al_2O_3-TPR < MoP, whereas the rates normalized per metal site (TOF) followed the trend: MoP/Al_2O_3-TPR < MoP < Ni_2P-CA < Ni_2P/Al_2O_3-TPR < Ni_2P/Al_2O_3-LT. Thus, the Ni_2P phase is intrinsically more active than MoP, although the overall activity is determined by the interplay between intrinsic activity and exposed active surface. The conversion of palmitic acid was achieved in a trickle bed flow reactor at varying temperature and residence times. The model reaction follows three different pathway: hydrodeoxygenation (HDO): $C_{15}H_{31}COOH \rightarrow C_{15}H_{31}CHO \rightarrow C_{16}H_{33}OH \rightarrow C_{16}H_{34}$; decarboxylation/decarbonylation (DCO): $C_{15}H_{31}COOH \rightarrow [C_{15}H_{31}CHO] \rightarrow C_{15}H_{32}$; and esterification: $C_{15}H_{31}COOH + C_{16}H_{33}OH \rightarrow C_{15}H_{31}COOC_{16}H_{33}$. The presence of Al_2O_3 increases the esterification rates due to relative high acidity, and makes the supported Ni_2P phase more selective towards CC bond cleavage than bulk Ni_2P or MoP/Al_2O_3-TPR.

1. Introduction

Due to environmental concerns, legislations have driven increasing contribution of biomass derived oil to fuel production. Therefore, refineries have to treat feedstocks with increasing concentrations of oxygen, which has to be removed in order to meet fuel requirements via hydrodeoxygenation (HDO) [1]. In this scenario, typical Co-Mo or Ni-Mo sulfide materials may not be the most appropriate catalysts due to their instability in the absence of sulfur or presence of high concentrations of water. In response to this challenge, many other materials have been tested ranging from supported metal catalysts to carbides and nitrides [2–6]. However, the application of transition metals reduces the possibility of blending biomass-derived oil with conventional fossil oil, because the high concentrations of sulfur and nitrogen in the latter could adversely impact on the performance of metal catalysts. Carbides and nitrides may be more active than conventional sulfide catalysts but are thermodynamically not stable and readily convert to the corresponding sulfides and oxides.

An interesting alternative to the materials mentioned before are phosphide of transition metals. These materials have been proven very active for hydrodesulfurization and, more importantly, have been found structurally stable under S- and O-containing conditions (although they may undergo surface modifications) [7–10].

* Corresponding authors. Fax: +49 89 28913544.
E-mail addresses: oliver.gutierrez@mytum.de (O.Y. Gutiérrez), johannes.lercher@ch.tum.de (J.A. Lercher).
[1] These authors contributed equally to this work.

http://dx.doi.org/10.1016/j.apcatb.2015.06.042
0926-3373/

Ni_2P (usually supported on SiO_2) has been studied in detail and has been reported as the most active phosphide for hydrodesulfurization (HDS) [7–11]. Fewer studies focused on HDO applications of phosphide materials are found in literature. Namely, bulk and SiO_2-supported phosphides of base metals (i.e., MoP, WP, Fe_2P, Co_2P, Ni_2P) have been shown to be active in the HDO of aromatic model compounds representative of lignin-based pyrolysis oil [12–15].

In this work, we have prepared bulk and alumina supported Ni_2P and MoP to explore their catalytic activity in the hydrodeoxygenation pathways of palmitic acid, which has been selected as an ideal model compound for bio-oil derived from, e.g., algae (third generation biofuel) [16,17]. The phosphides of Ni and Mo have been selected because these elements are two of the most common base metals in hydrotreating catalysts. Additionally, we have tested a few preparation methods in order to investigate the intrinsic properties of the phosphide phases and those of the carrier, as well as the possible synergy between them.

The effect of the transition metal was explored by comparing the activity of bulk MoP and Ni_2P. The latter was prepared with a modified synthesis procedure in order to obtain reasonable surface area. Furthermore, these two phosphides were also prepared on Al_2O_3 in order to determine the impact of the support on the physicochemical and kinetic properties of the phosphides. Finally, a study focused on Ni_2P-based materials was performed by comparing Ni_2P/Al_2O_3 samples prepared by two synthesis routes which lead to different features of the supported phase. An exploratory study of amorphous $AlPO_4$ applied as a support for Ni_2P and an optimization study for the synthesis of MoP/Al_2O_3 are presented in the Supporting information.

2. Experimental

2.1. Synthesis of the catalysts: temperature programmed reduction method (TPR)

Supported and unsupported nickel phosphide (Ni_2P) and molybdenum phosphide (MoP) were prepared by a temperature programmed reduction method [4] starting from the correspondent metal salt ($Ni(NO_3)_2{\cdot}6H_2O$ from Alfa Aesar or $(NH_4)_6Mo_7O_{24}{\cdot}4H_2O$ from Sigma–Aldrich) and $(NH_4)_2HPO_4$ (Sigma–Aldrich) dissolved in water. The solutions were prepared with a Ni/P molar ratio of 0.5 and a Mo/P molar ratio of 1. For unsupported catalysts, the solution was dried overnight at 383 K. The solid recovered was thermally treated in air at 773 K for 5 h (5 K min^{-1}) and afterwards in H_2 for 2 h at 923 K (heated at 5 K min^{-1} from room temperature to 573 K and at 2 K min^{-1} from 573 K to 923 K).

Ni_2P and MoP supported on Al_2O_3 (SCFa140 Sasol, porosity of 0.8 ml g^{-1}), were prepared through incipient wetness impregnation of the support with solutions of the metal salt ($Ni(NO_3)_2{\cdot}6H_2O$ or $(NH_4)_6Mo_7O_{24}{\cdot}4H_2O$) and $(NH_4)_2HPO_4$. The metal/P molar ratio was 0.5 whereas the content of metal was 10 wt.% in the initial solution. After drying at 383 K, the impregnated samples were then treated in air at 773 K for 5 h (5 K min^{-1}) and reduced in H_2 (up to 923 K for Ni_2P and 1073 K for MoP).

2.2. Synthesis of the catalysts: Low temperature method (LT)

Ni_2P supported on Al_2O_3, was synthesized with a method based on a low temperature treatment in flowing N_2 [30]. The sample was prepared by impregnating a certain amount of commercial Al_2O_3 (SCFa140 Sasol, porosity of 0.8 ml/g) with an aqueous solution of sodium hypophosphite ($NaH_2PO_2{\cdot}H_2O$, Sigma–Aldrich) and nickel chloride ($NiCl_2{\cdot}6H_2O$, Sigma–Aldrich). The Ni/P molar ratio was 0.5 and the metal content in the initial solution was 10 wt.%. After drying, the impregnated solid was heated in a fixed-bed rector to 573 K and kept for 1 h in flowing N_2 (30 ml min^{-1}). The material was cooled to room temperature under N_2 and was washed several times with deionized water to remove ionic impurities.

2.3. Synthesis of the catalysts: Citric acid method (CA)

A bulk Ni_2P sample was prepared following the TPR procedure but adding citric acid to the aqueous solution during the initial precipitation of the precursor salts [18,19]. Citric acid (CA) was added to the salt solution to give a 2:1CA:metal molar ratio. The solution was kept in an oil bath at 363 K for 3 days. The obtained gel was dried at 393 K for two days. Prior to calcination at 773 K, a thermal treatment step at 513 K for 1 h in air was required because of the high exothermicity of the decomposition of citric acid. During this step, the concentration of O_2 in N_2 was increased slowly from 1 vol.% to 20 vol.%. Further reduction in H_2 was performed for 2 h at 923 K. All the catalysts were passivated in a flow of 1 vol.% O_2 in N_2 (20 ml min^{-1}) to stabilize the catalysts for handling after reduction or inert treatment.

2.4. Characterization of the catalysts

N_2-physisorption isotherms were measured at liquid nitrogen temperature using a PMI automated sorptometer (Sorptomatic 1960). The samples were outgassed at 520 K for 2 h prior to N_2 adsorption. The data were employed to determine the texture of the oxide precursors, that is, surface area (BET analysis), pore volume, and pore size distribution (BJH method). X-ray powder diffraction (XRD) was performed with a Phillips/PANalytical's X'Pert PRO system (Cu Kα radiation, 0.154056 nm) operating at 45 kV and 40 mA. The XRD patterns were recorded using a scan speed of 1.08° min^{-1}. TEM images were recorded on a JEM-2010 JEOL transmission microscope operated at 120 kV. Samples were prepared by depositing drops of suspensions of the materials in ethanol on Cu grids with supporting carbon films. The statistical analysis of particle size was performed by measuring at least 300 particles per sample distributed in micrographs taken from different regions of the sample. The elemental contents of Mo, Ni and P in the materials were measured with a photometer Shimadzu UV-160. Carbon was quantified with an EURO EA (HEKA tech) instrument. CO chemisorption was applied to probe the metal sites by passing CO pulses (0.33 vol.% CO in He) through samples of the materials at 298 K. The CO uptake was monitored by a Balzers mass spectrometer ($m/z = 28$). Prior to the CO pulses, the passivated materials were activated in H_2 at 723 K for 2 h (Ni_2P/Al_2O_3 LT was reactivated at 573 K). The acidity was determined by temperature programmed desorption of NH_3 in a homemade vacuum-TPD set-up. After thermal treatment of the materials in hydrogen at 723 K, 1 mbar ammonia was adsorbed at 373 K for 1 h. The TPD was carried out up to 1043 K after outgassing physisorbed NH_3 for 4 h. The evolution of ammonia was monitored using a mass spectrometer ($m/z = 16$, Pfeiffer QMS 200).

2.5. Catalytic test

The HDO of palmitic acid was performed in a trickle fixed-bed reactor equipped with high pressure mass flow meters and a HPLC pump. A stainless steel, glass-coated tubular reactor was loaded with 0.04 g of catalyst (160–280 μm), diluted in 0.88 g of SiC. The entire reactor volume was packed with SiC (60–90 μm), which was held by quartz wool. Prior to activity tests, the phosphide catalysts were activated in a flow of 20 ml/min of H_2 for 2 h at 723 K to remove the passivated layer. Ni_2P/Al_2O_3 LT was activated for 2 h in H_2 at 573 K. The catalytic tests were performed at 4 MPa, contact times were between 0.3 and 2 h and temperature between 453 and 573 K. The contact time is defined as the inverse of the weight hour space velocity (WHSV), which is calculated as the mass flow

of palmitic acid divided by the mass of catalyst. The reactant mixture consisted of palmitic acid (1.2 wt.%) in dodecane and H_2 fed in downward and concurrent modes, keeping the molar ratio of H_2 to palmitic acid of 1000. Aliquots of 1 ml were periodically taken and analyzed by gas chromatography using a Shimadzu 2010 instrument with a HP-5 capillary column (30 m × 250 μm) and flame ionization detector. All samples used for the analysis were taken after 16 h on stream. Conversions and yields were calculated following classical definitions as shown in Eqs. (1)–(3), where C_{a_0}, and C_{a_f} are the concentrations of the reactant in the feed and in the effluent, and C_i is the concentration of the product i in the effluent. The concentrations of all products were determined by applying the corresponding response factors obtained from calibrations with pure compounds.

$$\text{Conversion}[\%] = \frac{C_{a_0} - C_{a_f}}{C_{a_0}} \times 100 \quad (1)$$

$$\text{Selectivity}_i[\%] = \frac{C_i}{C_{a_0} - C_{a_f}} \times 100 \quad (2)$$

$$\text{Yield}_i[\%] = \frac{\text{Conversion} \times \text{Selectivity}_i}{100} \quad (3)$$

3. Results and discussion

3.1. Exploratory studies

SiO_2 is usually preferred as a support for phosphides, because it does not interact strongly with phosphorous as Al_2O_3 does [20]. However, the carrier may play a catalytic role beyond only dispersing the phase with metal functionality and silica is largely inert. Thus, in this work we have taken alumina as a support. In order to reduce the migration of phosphorous towards alumina, we have attempted to support Ni_2P on amorphous aluminophosphate (AlPO), with the hypothesis that the P-saturated carrier would benefit the synthesis of the phosphide. We have succeeded in preparing Ni_2P/AlPO, as reported in the Supporting information. However, the activity of the material is very low due to a large collapse of the support during synthesis of the phosphide. Details of synthesis and results are presented in the Supporting information.

We followed reports in literature in order to prepare supported Ni_2P, which was successful. However, the synthesis of supported MoP was much more challenging as many attempts led to metallic Mo. Thus, an optimization study had to be done in order to prepare the desired MoP phase. Aiming to contribute to the knowledge of material preparation, we reported the optimization study in the Supporting information.

3.2. Physicochemical properties

An overview of the materials that were prepared in this study, the corresponding precursors and thermal treatments, are presented in Table 1. Note that the metal to P ratio used in the solutions impregnated on Al_2O_3 were 0.5. That is, phosphorous was present in excess in order to compensate for the losses due to the thermal treatment. All materials discussed below contained the Ni_2P or MoP phases as confirmed by XRD (vide infra). The metal to phosphorous molar ratios derived from the elemental analysis of the unsupported phosphides (Ni_2P, Ni_2P-CA, and MoP) (Table 2) were in perfect agreement with the expected stoichiometry of the phosphides. In contrast, the metal to phosphorous molar ratios of the supported phosphides, were all about 0.5, that is much lower than the stoichiometry of the phosphides (2 and 1 for Ni_2P and MoP, respectively). This was attributed to the well know migration of phosphorous into the Al_2O_3 support, leading to excess of phosphorous in the bulk of the material [20].

Fig. 1 shows the N_2 physisorption isotherms of the phosphide catalysts. The N_2-isotherm of the parent Al_2O_3 support and the pore size distributions are presented in the Supporting information. The wide hysteresis loop observed in the N_2-physisorption isotherm of Ni_2P-CA suggests a porous solid with a broad distribution of pore sizes due to the presence of relatively large cavities connected with narrower pores. Furthermore, a large contribution of micropores to the pore volume of the material is indicated by the large volume adsorbed at low relative pressures and confirmed by the high contribution of pores smaller than 5 nm to the porosity (Fig. S5 of the Supporting information). The supported catalysts (Ni_2P/Al_2O_3-LT, Ni_2P/Al_2O_3-TPR, and MoP/Al_2O_3) exhibit isotherms that correspond to the mesoporous structures of the bare Al_2O_3 support (type IV isotherms). The hysteresis loops of the phosphide catalysts broaden and shift to higher relative pressures with respect to pure alumina (presented in Fig. S4). These two effects reflect changes in the porous structure of the support during thermal treatment as observed in the pore size distributions of the Al_2O_3-containing materials (Supporting information). That is, compared to pure Al_2O_3 (with a pore size distribution centered at ~10 nm), the pore distributions of the supported catalysts broaden and are centered at smaller pore sizes. The isotherm of bulk MoP (Fig. 1B) indicates that the material has only macroporosity derived from the agglomeration of solid particles.

The surface area and pore volume of all materials are presented in Table 2. Compared to the bare Al_2O_3, the decrease in surface area of Ni_2P/Al_2O_3-TPR and MoP/Al_2O_3-TPR is larger than expected from the density increase after the deposition of the supported phase (from 144 $m^2\,g^{-1}$ in Al_2O_3 to 84 $m^2\,g^{-1}$ and 88 $m^2\,g^{-1}$ in Ni_2P/Al_2O_3-TPR and MoP/Al_2O_3-TPR, respectively). The pore volume also decreases dramatically (from 0.5 $cm^3\,g^{-1}$ in Al_2O_3 to 0.265 $cm^3\,g^{-1}$ and 0.225 $cm^3\,g^{-1}$ in Ni_2P/Al_2O_3-TPR, and MoP/Al_2O_3-TPR, respectively). This confirms that the pore structure of alumina changes during the thermal treatments as discussed above. In contrast, the decrease of surface area in Ni_2P/Al_2O_3-LT (130 $m^2\,g^{-1}$, compared to 144 $m^2\,g^{-1}$ of pure alumina) corresponds to what is expected from an ideal phosphide deposition. Thus, a more homogeneous distribution of the supported phase inside the pores of the carrier is obtained in Ni_2P/Al_2O_3-LT (which would, in turn, decrease the pore volume from 0.52 $cm^3\,g^{-1}$ in Al_2O_3 to 0.295 $cm^3\,g^{-1}$). This is well in line with the minor shift of the hysteresis loop accompanied by a small broadening in the N_2-isotherm of Ni_2P/Al_2O_3-LT discussed above.

Bulk MoP exhibits very low surface area (6 $m^2\,g^{-1}$) as expected from the lack of microporosity and mesoporosity. In stark contrast, Ni_2P-CA had an outstanding surface area (230 $m^2\,g^{-1}$) and porosity (0.197 $cm^3\,g^{-1}$) which has been related to the high carbon content of the material. This carbon, residue from the synthesis, seems to host the high microporosity observed in the pore distribution in addition to mesoporosity (vide supra).

The X-ray diffractograms of all materials are presented in Fig. 2 (Ni_2P-containing catalysts) and Fig. 3 (MoP-containing catalysts). Only the phases Ni_2P (ICOD: 01-074-1385) and MoP (ICOD: 00-024-0771) were identified in the materials. As expected, the crystallinity depended on the presence of support and the synthesis temperature. The bulk materials exhibited sharp and intense reflections, whereas the supported phosphides exhibited small reflections, especially MoP/Al_2O_3 and Ni_2P/Al_2O_3-LT where the small reflections of the phosphide phases strongly overlap with those of alumina. However, direct comparison of the diffractogram of the catalysts with that of pure alumina (Fig. 3) indicates that the expected phosphides phases are present in the supported catalysts. The material Ni_2P/Al_2O_3-LT was treated at high temperature in order to corroborate the formation of the phosphide phase. The X-ray diffractogram of this sample is shown in the Supporting information.

Table 1
List of catalysts used in this work, corresponding precursors, proportions used in the initial solutions and thermal treatments.

Catalyst	Metal/P molar ratio	Metal precursor	Phosphorus precursor	Reduction
Ni_2P	1/2	$Ni(NO_3)_2{\cdot}6H_2O$	$(NH_4)_2HPO_4$	2 h 923 K H_2
Ni_2P-CA	1/2	$Ni(NO_3)_2{\cdot}6H_2O$	$(NH_4)_2HPO_4$	2 h 923 K H_2
MoP	1	$(NH_4)_6Mo_7O_{24}{\cdot}4H_2O$	$(NH_4)_2HPO_4$	2 h 923 K H_2
Ni_2P/Al_2O_3-LT	1/2	$NiCl_2{\cdot}6H_2O$	$NaH_2PO_2{\cdot}H_2O$	1 h 573 K N_2
Ni_2P/Al_2O_3-TPR	1/2	$Ni(NO_3)_2{\cdot}6H_2O$	$(NH_4)_2HPO_4$	2 h 923 K H_2
MoP/Al_2O_3-TPR	1/2	$(NH_4)_6Mo_7O_{24}{\cdot}4H_2O$	$(NH_4)_2HPO_4$	2 h 1073 K H_2

Table 2
Physicochemical properties of Al_2O_3 and phosphide catalysts.

Catalyst	Elemental analysis			Texture		Phosphide properties
	Metal, wt.%	P, wt.%	Metal/P, Molar ratio	BET Surface area, $m^2\ g^{-1}$	Pore volume, $cm^3\ g^{-1}$	Particle size, nm
Al_2O_3	–	–	–	144	0.52	–
Ni_2P/Al_2O_3-TPR	6.5	7.8	0.44	83.9	0.265	24.3[b]
Ni_2P/Al_2O_3 -LT	6.2	6.3	0.52	129.9	0.295	14[c]
Ni_2P	61.4	22.4	1.45	<5	n.d.[d]	132.4[b]
Ni_2P-CA[a]	50.2	12.5	2.10	229.6	0.197	49.0[b]
MoP/Al_2O_3-TPR	7.4	5.0	0.48	88.5	0.225	12[c]
MoP	65.9	21.0	1.01	5.9	n.d.	29.2[b]

[a] The content of C in Ni_2P-CA is 25.6 wt.%
[b] Obtained from XRD analysis using the Scherrer equation.
[c] Obtained from TEM analysis.
[d] n.d. not determined.

The crystal sizes derived from the X-ray diffractograms are reported in Table 2, whereas particle sizes of MoP/Al_2O_3 and Ni_2P/Al_2O_3-LT, were calculated from a statistical analysis of TEM micrographs (Fig. 4). The average size determined from the analysis of TEM images is larger than expected from the tiny reflections of the XRD diffractograms. This disagreement is likely due to overestimation of the size from TEM images, where small phosphide particles would escape from detection. MoP forms smaller particles than Ni_2P, i.e., 29 nm for MoP and 132 nm for Ni_2P. On alumina (MoP/Al_2O_3-TPR and Ni_2P/Al_2O_3-TPR) MoP, and Ni_2P particles are 13 nm and 24 nm, respectively. The low temperature method leads to smaller Ni_2P particles than the typical TPR approach. That is, 13.5 nm in Ni_2P/Al_2O_3-LT, and 24 nm in Ni_2P/Al_2O_3-TPR.

The use of citric acid during the synthesis reduces the crystal size (as derived from XRD) of Ni_2P from 132 nm (Ni_2P) to 49 nm (Ni_2P-CA). This is in excellent agreement with several studies, where the addition of citric acid allows obtaining active phases with high dispersion and activity. This is due to the chelating properties of citric acid, which forms complexes with the catalyst precursors slowing the sintering of active phases [21–23].

Fig. 4 shows selected TEM micrographs of the phosphide particles in the materials. The images confirm that the typical TPR method leads to larger Ni_2P particles than the low temperature approach. Interestingly, the Ni_2P particles in Ni_2P/Al_2O_3-LT are smaller than on Ni_2P/Al_2O_3-TPR, however, they form large assemblies as presented in Fig. 4. This has important implication for

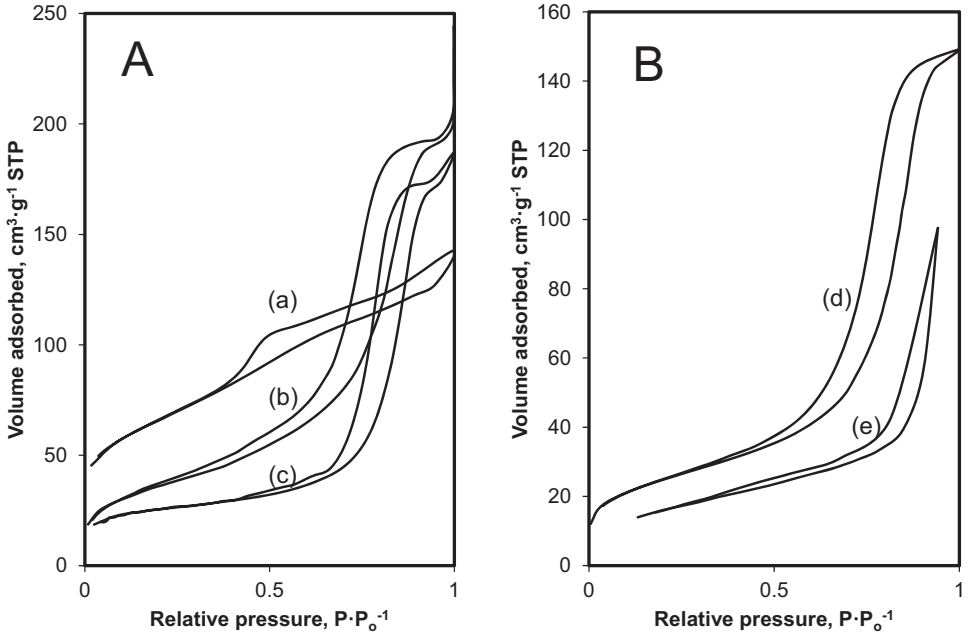

Fig. 1. N_2 physisorption isotherms of (A) Ni-based and (B) Mo-based phosphide catalysts: Ni_2P CA (a); Ni_2P/Al_2O_3 LT (b); Ni_2P/Al_2O_3 TPR (c); MoP/Al_2O_3 TPR (d); MoP (e).

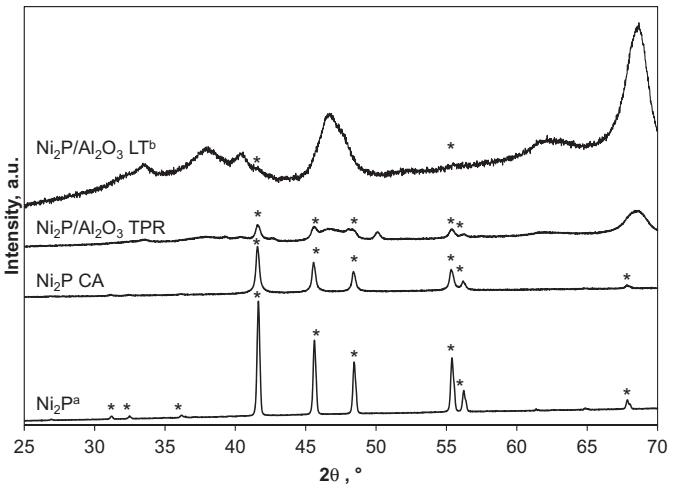

Fig. 2. X-ray diffractograms of Ni_2P-based catalysts. (*) Ni_2P; the diffractions not labeled correspond to Al_2O_3. [a] Multiplied by a factor of 0.3. [b] Multiplied by a factor of 5.

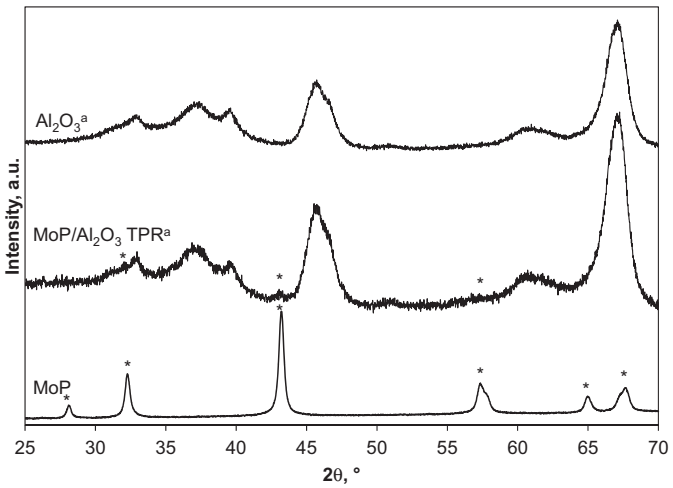

Fig. 3. X-ray diffractograms of MoP-based catalysts and Al_2O_3. (*) MoP; the diffractions not labeled correspond to Al_2O_3. [a] Multiplied by a factor of 10.

catalytic activity (vide infra). The micrographs of Ni_2P-CA demonstrate that the phosphide crystals are embedded in a carbonaceous structure, which increases the porosity of the catalysts and the dispersion of the Ni_2P particles. Figs. 2 (XRD) and 4 (TEM), show that the particle size in the Ni_2P-CA is much smaller than on Ni_2P. Thus, the role of citric acid is twofold, it prevents the Ni_2P particles from sintering and the residual carbon supports these particles. The drawback of this C-Ni_2P system is that the phosphide surface is covered by carbon (vide infra) to extents that must depend on the synthesis conditions. The TEM images also confirm smaller particle size for MoP than Ni_2P in bulk and supported materials.

A complete discussion of the properties of the phosphides studied in this work requires the determination of metal and acid site concentrations. These properties are assessed by adsorption of CO and TPD of NH_3. The concentration of both probe compounds adsorbed by the materials is presented in Table 3. Among unsupported materials, the concentration of adsorbed CO is much higher in MoP (10 $\mu mol\, g^{-1}$) than in Ni_2P-CA (0.23 $\mu mol\, g^{-1}$), in contrast to the surface area trend determined by N_2 physisorption. This is a confirmation of the strong effect of residual carbon, which covers a large proportion of metal surface on the latter. Among supported catalysts, which exhibit higher CO uptake than Ni_2P-CA but lower than MoP, the concentration of adsorbed CO increases as follows: Ni_2P/Al_2O_3-LT (0.29 $\mu mol\, g^{-1}$) < Ni_2P/Al_2O_3-TPR (0.61 $\mu mol\, g^{-1}$) <

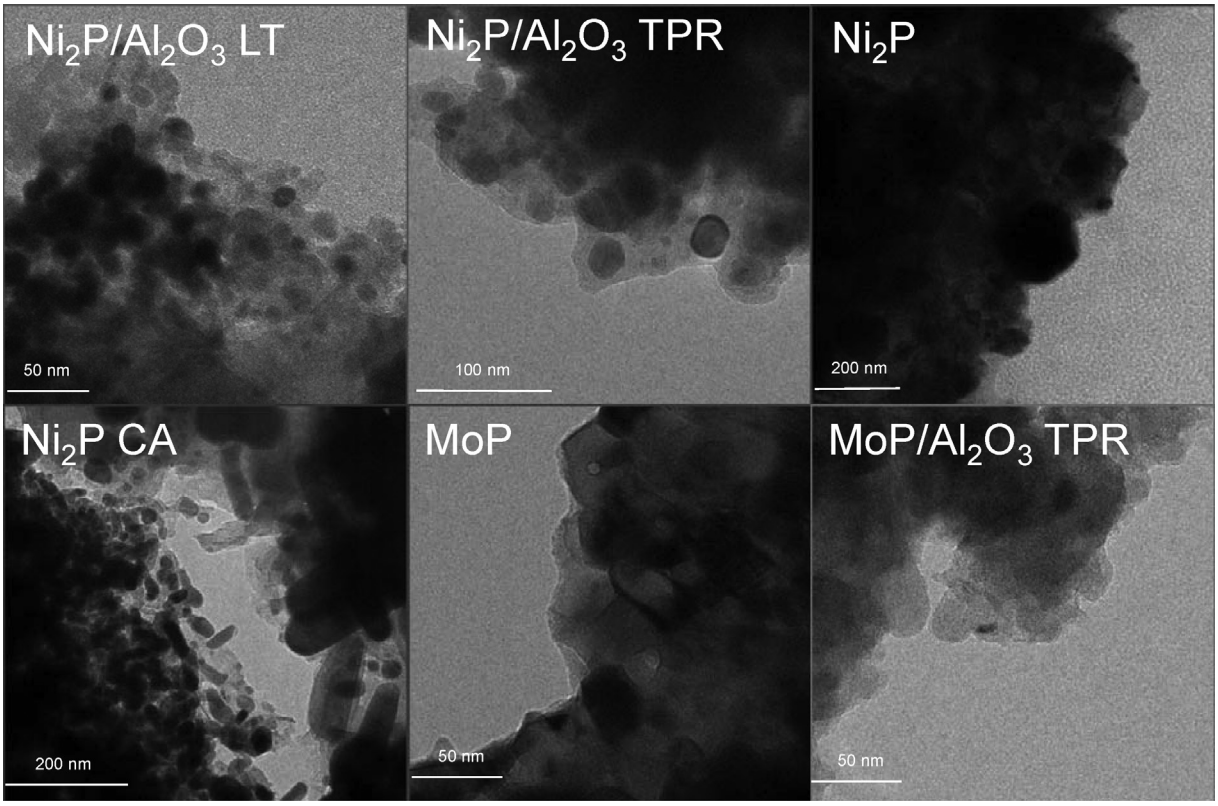

Fig. 4. Representative TEM micrographs of the phosphide catalysts.

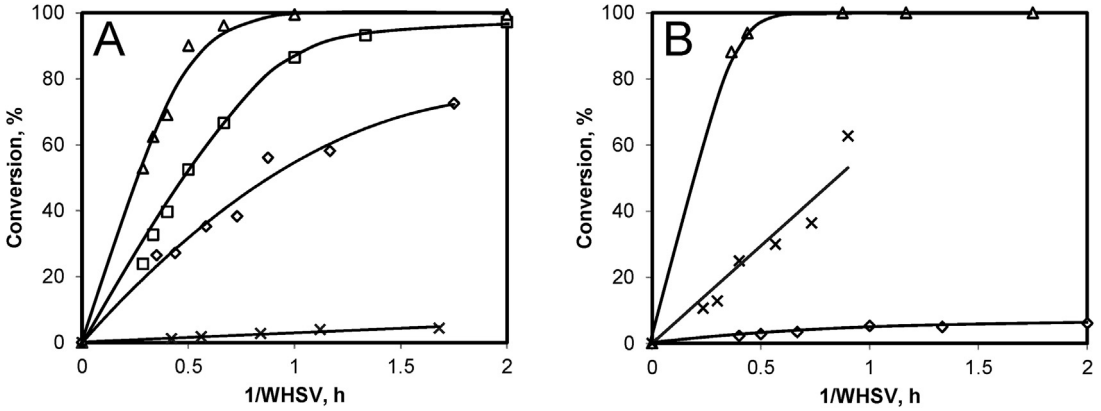

Fig. 5. Effect of residence time on the conversion of palmitic acid at varying residence time at 573 K, and 4 MPa H_2. (A) Ni-based phosphides: Ni_2P (×), Ni_2P-CA (◊), Ni_2P/Al_2O_3-LT (□), and Ni_2P/Al_2O_3-TPR (Δ); (B) Mo-based catalysts and alumina: MoP (Δ), MoP/Al_2O_3-TPR (x), Al_2O_3 (◊).

Table 3
Concentration of CO or NH_3 adsorbed on the phosphide catalysts as determined by pulse and TPD experiments, respectively.

Catalyst	CO, μmol g^{-1}	NH_3, mmol g^{-1}
Ni_2P-CA	0.23	0.077
MoP	10.1	0.040
Ni_2P/Al_2O_3-LT	0.29	0.244
Ni_2P/Al_2O_3-TPR	0.61	0.190
MoP/Al_2O_3-TPR	6.40	0.191
Ni_2P	–	0.019

MoP/Al_2O_3-TPR (6.4 mmol g^{-1}). The total acidity of the bulk materials is one order of magnitude lower than that of the supported catalysts. The materials obtained by TPR have the same acid site concentration of 0.19 mmol g^{-1}, whereas Ni_2P/Al_2O_3-LT has an acid site concentration of 0.244 mmol g^{-1}. The parent alumina has an acid site concentration of 0.1 mmol g^{-1}. That is, lower than that of the supported phosphide catalysts. This is attributed to the formation of aluminum phosphate due to the migration of phosphorous towards the support. As reference, the $AlPO_4$ material synthesized in exploratory experiments exhibits an acidity of 0.292 mmol g^{-1} (see the Supporting information).

3.3. Catalytic tests at constant temperature and reaction network

The catalytic activity of bulk and supported phosphides is investigated in the conversion of palmitic acid under hydrodeoxygenation (HDO) conditions at constant temperature or constant residence time. Fig. 5 shows the conversion of palmitic acid at 573 K, 4 MPa, and varying residence time. Table 3 reports rate constants (k) at 573 K assuming first order kinetics. The bare Al_2O_3 support and the bulk Ni_2P sample exhibit conversions of palmitic acid below 10% with k values of 0.05 h^{-1} and 0.04 h^{-1}, respectively, at 573 K. The activity of the other catalysts increases following the trend: MoP/Al_2O_3 ($k = 0.57\ h^{-1}$) < Ni_2P-CA ($k = 0.66\ h^{-1}$) < Ni_2P/Al_2O_3-LT ($k = 1.92\ h^{-1}$) < Ni_2P/Al_2O_3-TPR ($k = 2.86\ h^{-1}$) < MoP ($k = 5.64\ h^{-1}$). The products of the reaction are hexadecanal (in trace concentrations), hexadecanol, palmityl palmitate, hexadecane, and pentadecane. The yields of these products, along with residence time on Ni_2P- and MoP-containing catalysts, are presented in

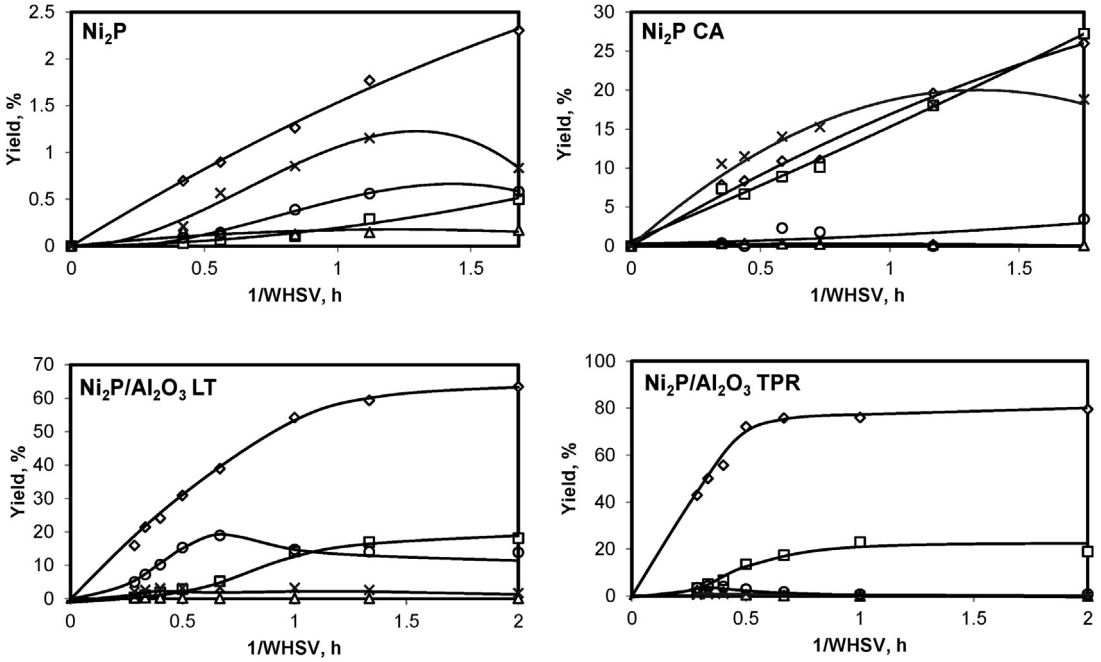

Fig. 6. Effect of residence time on the yields of pentadecane (◊), hexadecane (□), hexadecanal (Δ), hexadecanol (×) and palmityl palmitate (○) at different residence times on Ni_2P-based catalysts.

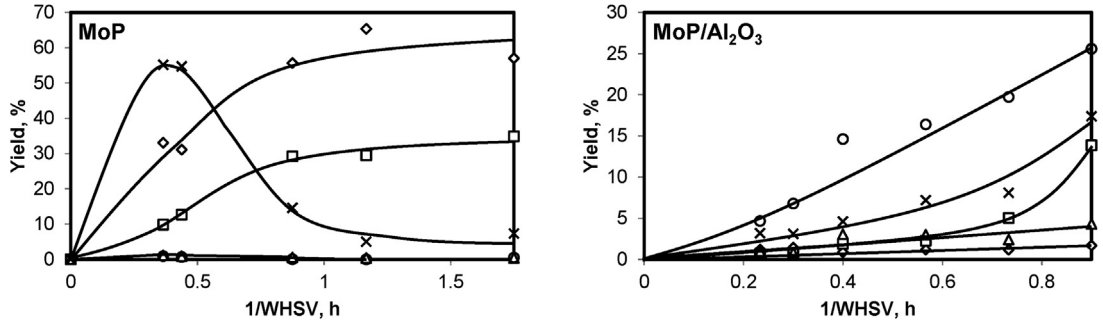

Fig. 7. Effect of residence time on the yields of pentadecane (◊), hexadecane (□), hexadecanal (Δ), hexadecanol (×) and palmityl palmitate (○) at different space times on MoP-based catalysts.

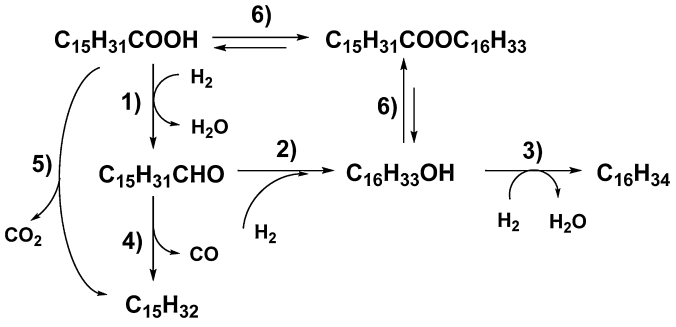

Fig. 8. Proposed reaction network; the reaction steps are hydrogenolysis (1), hydrogenation (2), dehydration-hydrogenation (3), decarbonylation (4), decarboxylation (5), and esterification (6).

Figs. 6 and 7, respectively (yield versus conversion plots are presented in the Supporting information).

The product distributions on the most active catalysts (on, i.e., Ni_2P/Al_2O_3-TPR, and MoP) show that the alkanes are final products of the reaction at the experimental conditions (steady yields at full conversion of palmitic acid), as intuitively expected. On the other hand, the yields on materials with low activity (Al_2O_3, Ni_2P) allow concluding that hexadecane is also a secondary product as its concentration increases exponentially with increasing residence time. Pentadecane behaves as a primary product as its concentration increases linearly at short residence times. Hexadecanol, palmityl palmitate, and hexadecanal are products of the reaction. If present in quantitative amounts, hexadecanal behaves as a primary product. Hexadecanol and palmityl palmitate behave as primary products on most catalysts. However, their secondary nature is revealed on phosphides with very low activity.

The analysis of the product distribution in dependence of residence time, and conversion of palmitic acid, allows adapting the reaction networks proposed for the HDO of microalgae oil on Ni-based catalysts and methyl laurate on phosphides supported on silica to the HDO of palmitic acid on phosphides [16,17]. The resulting network is shown in Fig. 8. The first step of a route without carbon losses is the hydrogenolysis of the carboxylic group in palmitic acid to hexadecanal. This intermediate rapidly converts via hydrogenation to hexadecanol, which yields hexadecane via consecutive dehydration to a terminal alkene, and hydrogenation to hexadecane. The alkene is not observed in this study (likely due to fast hydrogenation under high hydrogen partial pressure); hence, it is not included in the reaction network of Fig. 8. Pentadecane is produced either by decarbonylation of hexadecanal or by direct decarboxylation of palmitic acid. Another parallel reaction is the rapid esterification reaction between hexadecanol and palmitic acid to palmityl palmitate.

On bulk Ni_2P-CA and MoP, hexadecanal and palmityl palmitate are produced only in trace concentrations. Hexadecanol is the main product at short residence times whereas alkanes dominate at long residence times. Ni_2P-CA produces hexadecane and pentadecane in similar concentrations, whereas MoP favors the formation of pentadecane over hexadecane. The supported catalysts lead to increased yields of palmityl palmitate and low concentrations of hexadecanol. These observations imply that hydrogenolysis of palmitic acid to hexadecanal is slow and further conversion of the latter is fast. In turn, hydrogenation of hexadecanal to hexadecanol is faster than decarboxylation and decarbonylation (the sum of hexadecanol and hexadecane yields is larger than the pentadecane yield). Further transformation of the alcohol to hexadecane is relatively slow.

On the supported catalysts, the yields of hexadecanal are also very low, which confirms the slow hydrogenolysis of palmitic acid towards hexadecanal compared to further reaction steps. In the presence of Al_2O_3, the yields of hexadecanol are drastically reduced compared to bulk phosphides. Conversely, the yields of palmityl palmitate significantly increase. This is a consequence of the esterification of hexadecanol and palmitic acid, which is catalyzed by Al_2O_3 (bare Al_2O_3 produced mainly palmityl palmitate as shown in the Supporting information). On supported Ni_2P (Ni_2P/Al_2O_3-LT, Ni_2P/Al_2O_3-TPR), the high pentadecane yields indicated that decarbonylation/decarboxylation is preferred over hydrogenation. This is attributed to an effect of supporting the phosphide phase, because pure Al_2O_3 did not lead to important pentadecane production. Furthermore, esterification is concluded to be faster than the hydrogenation steps leading to hexadecane as its yield increases only when the concentrations of palmitic acid are very low, and therefore fast decomposition of palmityl palmitate is allowed. MoP/Al_2O_3 leads to low pentadecane yield, which indicates low decarboxylation/decarbonylation selectivity. Furthermore, substantial concentrations of hexadecanol and palmityl palmitate (found as the main products in the whole conversion range) suggest that on this catalyst, dehydration and hydrogenation of the alcohol is much slower than esterification.

In order to illustrate the differences among Ni_2P-containing materials (discussed below), Fig. 9 shows a direct comparison of the product distribution at similar conversions, constant temperature and residence time (553 K, 1 h). On the supported phosphides, large concentrations of palmityl palmitate are obtained (more on Ni_2P/Al_2O_3-LT than on Ni_2P/Al_2O_3-TPR), whereas very little of this ester is formed on Ni_2P-CA. In contrast, this bulk material yields hexadecanol as the main product (at around 50% conversion of palmitic acid), whereas the Al_2O_3-supported phosphides yield only minor concentrations of this alcohol. Another significant difference is that the supported materials produce low concentrations of hexadecane but very high concentrations of pentadecane while the unsupported Ni_2P-CA leads to higher hexadecane selectivity

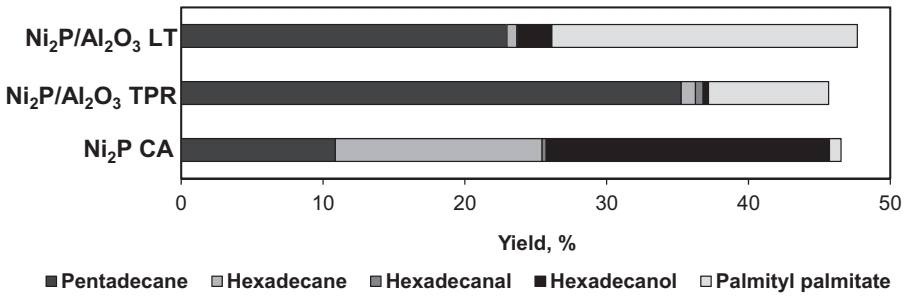

Fig. 9. Comparison of the product yields of Ni_2P-based catalysts at similar conversions, 553 K, 40 MPa, and 1 h.

compared to pentadecane. The hexadecanal yields were very low on all materials.

3.4. Catalytic tests at varying temperatures and kinetic parameters

The HDO activity of the phosphide catalysts is also explored at varying temperatures (Fig. 10). On all Ni_2P catalysts (Ni_2P-CA, Ni_2P/Al_2O_3-TPR, and Ni_2P/Al_2O_3-LT), surprisingly, almost the same conversions of palmitic acid was observed in the range of 473–573 K. Therefore, the observations done at 573 K and varying residence time hold true for the whole temperature range. That is, bulk Ni_2P-CA produces small concentrations of palmityl palmitate and hexadecanal, considerable concentrations of hexadecanol (main product below 573 K), and similar concentrations of hexadecane and pentadecane. This implies that on Ni_2P-CA, the rate of hydrogenolysis of the acid is much faster than esterification, whereas the decarboxylation of the acid (or decarbonylation of the aldehyde) and hydrogenation of the intermediate aldehyde have similar rates. In contrast, supporting the Ni_2P phase on Al_2O_3, considerably decreases the selectivity to hexadecanol, hexadecanal, and hexadecane yielding pentadecane and palmityl palmitate as main products. On Ni_2P/Al_2O_3-TPR, pentadecane is the most abundant product (i.e., decarbonylation/decarboxylation is the fastest pathway), whereas on Ni_2P/Al_2O_3-LT, the yield of palmityl palmitate equals that of pentadecane below 553 K (decarbonylation/decarboxylation, and esterification have very similar rates) Fig. 11.

The HDO activity of bulk MoP is much higher than that of MoP/Al_2O_3 in the whole temperature range. In turn, the former is more active and the latter less active than all Ni_2P catalysts. The product distribution is shown in Fig. 12. MoP yields large concentrations of hexadecanol, which is the major product in most of the tested temperature range. The offset for hexadecane and pentadecane production is 533 K, both alkanes being produced at similar rates. On MoP/Al_2O_3-TPR, palmityl palmitate is the predominant product followed by hexadecanol. The offset for the production of the alkanes was 553 K. These observations indicate that decarbonylation of hexadecanal and dehydration-hydrogenation of hexadecanol, are much slower than hydrogenolysis of palmitic acid (and slower than esterification on MoP/Al_2O_3-TPR).

Results of the experiments at varying temperatures allow determining the apparent activation energies (E_a) shown in Table 4. As expected from the comparable conversions on the studied temperature range, very similar E_a values were found on all Ni_2P catalysts, i.e., 112–120 kJ mol^{-1}. The E_a of MoP and MoP/Al_2O_3-TPR was 56 kJ mol^{-1} and 84 kJ mol^{-1}, respectively. Table 4 also presents the initial rates at 573 K per gram of material in the catalysts. The initial rates follow the same trends as the conversion and k values, i.e., MoP/Al_2O_3-TPR < Ni_2P-CA < Ni_2P/Al_2O_3-LT < Ni_2P/Al_2O_3-TPR < MoP. In turn, these trends correspond to the concentration of metal sites probed by CO adsorption within each phosphide series, i.e., MoP/Al_2O_3-TPR < MoP, and Ni_2P < Ni_2P-CA < Ni_2P/Al_2O_3-LT < Ni_2P/Al_2O_3-TPR (Table 3). This confirms, as expected, that the first, and rate limiting step of the reaction, occurs on the surface of either MoP or Ni_2P (regardless of the involvement of active sites on Al_2O_3). The activity of Ni_2P/Al_2O_3-LT is lower than expected from the small particle size of the supported phosphide likely due to the agglomeration of the Ni_2P particles (detected by TEM), which reduces the proportion of exposed metal area as shown by the trend of CO uptake. The rates normalized per active site as determined by CO adsorption (turnover frequencies, TOF) follow the trend: MoP/Al_2O_3-TPR < MoP < Ni_2P-CA < Ni_2P/Al_2O_3-

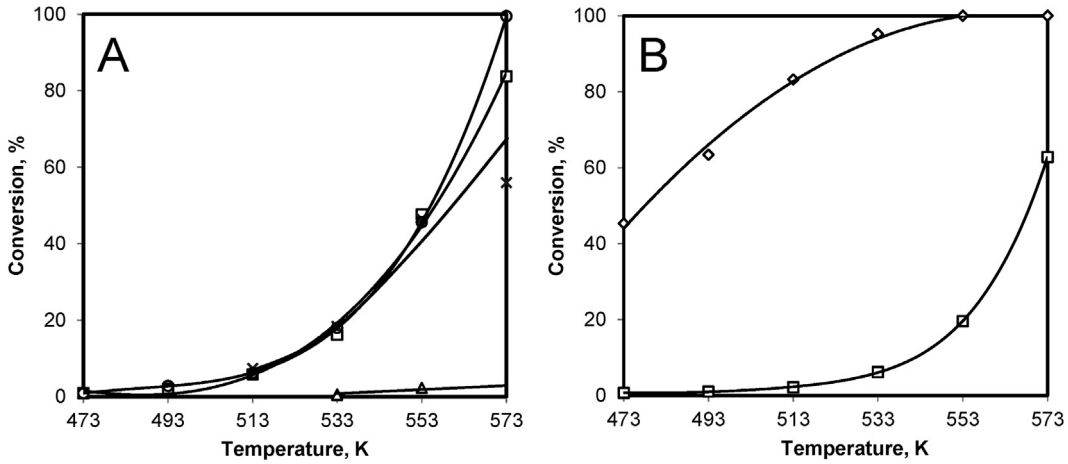

Fig. 10. Effect of temperature on the conversion of palmitic acid at varying temperatures at WHSV 1 h^{-1}, and 4 MPa H_2. (A) Ni-based phosphides: Ni_2P (Δ), Ni_2P CA (×), Ni_2P/Al_2O_3 LT (□), Ni_2P/Al_2O_3 TPR (○): (B) Mo-based catalysts. MoP (◊), MoP/Al_2O_3 TPR (□).

TPR < Ni_2P/Al_2O_3-LT. These values show that Ni_2P is intrinsically more active than MoP. Furthermore, the TOF values on Ni_2P catalysts increase with decreasing particle size. Bulk MoP is an outstanding material because it exhibits higher CO chemisorption and TOF than the supported counterpart (in contrast to the Ni_2P series). At present we speculate that this difference is related to the absence of any carrier (Al_2O_3 in the case of the supported catalysts or the carbon structure for Ni_2P-CA), i.e., support-active phase interphase. This could minimize the differences between the geometric surface (what correspond to the crystal size) and the exposed surface (effectively available for adsorption).

3.5. On the role of support and phosphide phase in the hydodeoxygenation of palmitic acid

Ni_2P and MoP are metal rich phosphides. MoP consists of hexagonal layers of P with Mo in the trigonal prismatic positions. All Mo atoms are equivalent as well as all P atoms [7,8]. Ni_2P has two kinds of metal sites, distorted tetrahedron (four coordinate), and square pyramid (five coordinate). All P atoms are located in face-capped trigonal prisms, but there are also two kinds of P sites depending on their coordination with 4- and 5-coordinate Ni atoms [7,8]. The net charges of metal and phosphorous atoms depend on their position within the phosphide structure. In MoP the charges of Mo and P are just slightly positive and negative, respectively, whereas in Ni_2P Ni is slightly positive or negative and P slightly positive [9]. Hence these phosphides have covalent bonding and metal-like character.

Phosphorous exerts electronic effects on the metal atoms, which have been evoked as ligand effects (Ni → P charge transfer) [24,25]. Moreover, structural effects of P on the metals result from increasing the distances between the metal sites, compared to the pure metal structure [24,26]. These effects result in lower reactivity than the corresponding pure transition metals, and improved stability towards phase transitions (e.g., towards sulfides in S-containing environments). In turn, P atoms may hold and provide H atoms for hydrogenation and hydrogenolysis of reactants adsorbed at the metal atoms.

Apart from the metal sites (metal atoms or metal-P ensembles), OH groups have been identified at the surface of phosphides as a result of strong P—O bonds [27,28]. These OH groups have been attributed with acidic properties giving bifunctional character to phosphide catalysts. On the other hand, hydrogenolysis and hydrogenation selectivities have been associated to varying concentration of OH groups [29].

The differences in activity between Ni_2P and MoP arise from different intrinsic rates of the rate determining steps for the hydrogenolysis of the adsorbed intermediates. According to the TOF values observed in this work, Ni_2P is intrinsically more active than MoP. This is the same case for the parent pure transition metals, i.e., Ni is a better hydrogenolysis catalyst than Mo.

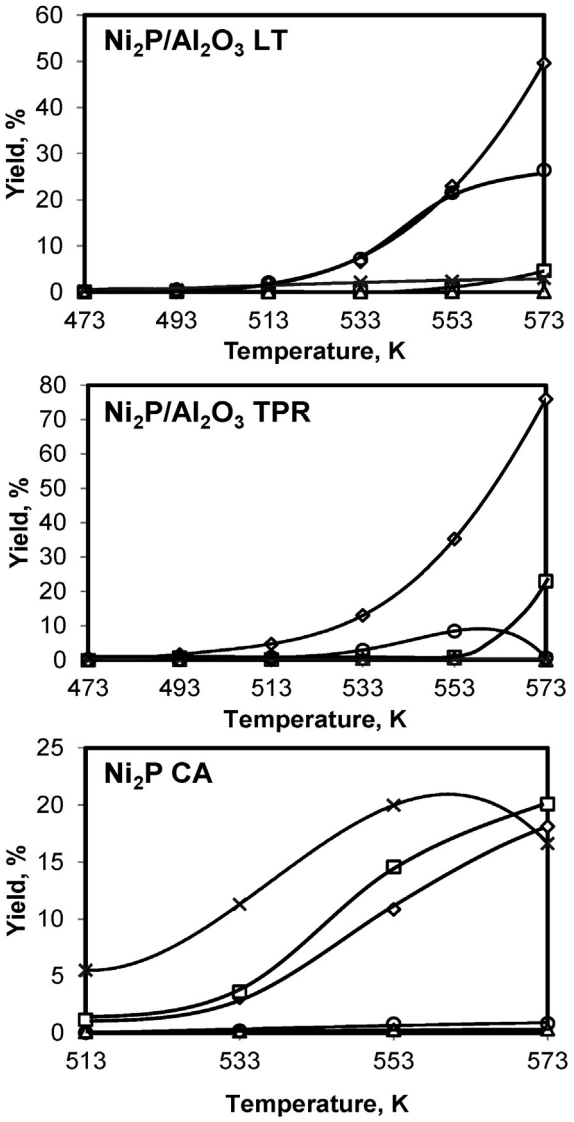

Fig. 11. Effect of temperature on the yields of pentadecane (◊), hexadecane (□), hexadecanal (Δ), hexadecanol (×) and palmityl palmitate (○) on Ni_2P-based catalysts at varying temperature, WHSV 1 h^{-1}, and 4 MPa H_2.

Following this analogy, the adsorption of the carboxyl group on the metal surface may occur on heterolytic or homolytic dissociation of the OH group deriving a bidentate structure via the carboxylate oxygen atoms (carboxylate intermediate) [30,31]. Subsequent hydrogen additions would lead to the hydrogenolysis of one C—O

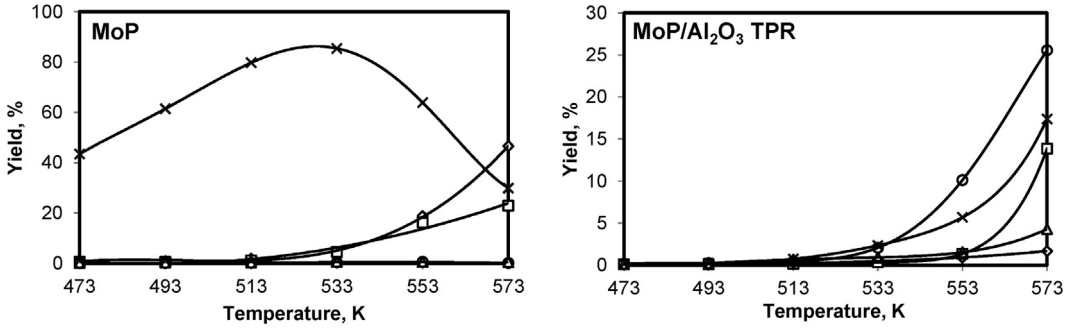

Fig. 12. Effect of temperature on the yields of pentadecane (◊), hexadecane (□), hexadecanal (Δ), hexadecanol (×) and palmityl palmitate (○) on MoP-based catalysts at varying temperature, WHSV 1 h^{-1}, and 4 MPa H_2.

Table 4
Kinetic parameters for the conversion of palmitic acid on selected materials.

	k[a], h^{-1}	E_a, KJ mol^{-1}	Initial rate[b], mmol $(g_{cat}\ h)^{-1}$	TOF[c], $h^{-1} \times 10^3$
Al_2O_3	0.05	n.d.[d]	0.20	n.d.
Ni_2P/Al_2O_3-TPR	2.86	117	7.23	11.8
Ni_2P/Al_2O_3-LT	1.92	112	4.89	16.8
Ni_2P	0.04	n.d.	0.092	n.d.
Ni_2P-CA	0.66	120	2.44	10.5
MoP/Al_2O_3-TPR	0.57	84	1.25	0.20
MoP	5.64	56	14.28	1.41

[a] Calculated at 573 K assuming a first order reaction.
[b] Calculated at 573 K at conversion below 20%.
[c] Calculated at 573, dividing the initial rate by the concentration of adsorbed CO reported in Table 3.
[d] n.d. not determined.

bond towards a η_1(C)-acyl intermediate and then an adsorbed aldehyde [32].

The aldehyde (hexadecanal), produced from the hydrogenolysis of the acid (palmitic acid), adsorbs again on the phosphide, metal-like, phase yielding aldehyde or acyl intermediates. Those intermediates may lead to hydrogenation (hexadecanol) or decarbonylation (pentadecane) [33,34]. The preference for one pathway or another also depends on the intrinsic properties of the phosphide. A simple analogy with the pure transition metals would indicate that Ni_2P is more active for decarbonylation than MoP as Ni has a much higher activity than Mo for CC bond cleavage [35]. Although this analogy is questionable because the electronic properties of MoP differ substantially from those of Mo (as in the case of Mo carbide and nitride [36]), lower decarbonylation has indeed been observed on MoP, compared to Ni_2P [17]. In line with this, the yields of pentadecane on Ni_2P series are higher, as a function of temperature and contact time, than on the MoP catalysts.

Hexadecanol reacted with palmitic acid to palmityl palmitate via esterification. This reaction occurred on the acid sites of Al_2O_3 as indicated by the facts that palmityl palmitate is the main product on alumina, and that it is formed with large yields on the alumina-supported phosphides. Accordingly, the concentration of acid sites is much larger on the catalysts with Al_2O_3. In contrast, unsupported phosphides exhibit a much lower acidity, which leads to very low esterification rates. Thus, in the absence of Al_2O_3, palmitic acid is unable to react with hexadecanol, which is the main C16 product with the bulk phosphides within large ranges of palmitic acid conversion. The mechanism of esterification is the same with heterogeneous and homogenous catalysts [37]. That is, the interaction of the carbonyl group in the acid (palmitic acid) activates the carbon in the carbonyl as an electrophile, which interacts with the hydroxyl group in an alcohol (hexadecanol). As a result of rearrangement, a hydroxyl group of the adsorbed complex converts into water, which is a good leaving group. In the final step, the ester (palmityl palmitate) desorbs regenerating the acid site. Ni_2P/Al_2O_3-LT produces more ester than Ni_2P/Al_2O_3-TPR, likely due to the higher concentration of acid sites of the former as determined from NH_3 TPD. In turn, the higher acid site concentration might be due to lower dehydration of the alumina at the relatively mild conditions of the low temperature approach. At high temperatures used for Ni_2P/Al_2O_3-TPR, fewer acidic sites are expectable.

The acidity of alumina also plays an important role in the transformation of hexadecanol to hexadecane as concluded by the accumulation of the alcohol (without ester formation) on bulk phosphides. However, it is not a single site in alumina, which catalyzed this step (pure alumina produced only trace amounts of hexadecanol and hexadecane). Thus, a synergy has to exist between the acid sites of the Al_2O_3 support and the metal sites on the supported phosphide phases as concluded for the Ni catalysts supported on metal oxides or zeolites [38,39]. This synergy consists of consecutive alcohol dehydration on alumina (a well-studied reaction [40]) and hydrogenation of the resulting alkene on the phosphide phase. Moreover, the hydrogenation on the phosphide phase is much faster than dehydration as hexadecene was not detected.

The yield of hexadecane on supported phosphides increases with high conversions of palmitic acid at high residence times or at high temperatures. This is attributed to the decrease of the surface coverage of palmitic acid, which increases the possibility that hexadecanol reacts with the acid sites on alumina yielding the intermediate hexadecene. Note however, that the phosphide phase is not at all unreactive towards the production of hexadecane (consecutive dehydration and hydrogenation). Ni_2P-CA produces similar concentrations of pentadecane and hexadecane, whereas on MoP and Ni_2P, the yield of hexadecane remains low but increases rapidly with increasing residence time and temperature. This feature has to be highlighted as it contrasts the observations done for HDO of fatty acids on Ni supported on not-acidic materials, where alcohol hydrogenation does not occur [39]. In turn, the implication of this pathway (hexadecanol to hexadecane) on phosphides is that the low acidity detected by NH_3-TPD indeed catalyzes some steps of the reaction network to some extent. Remarkably, these acid sites of bulk phosphides are able to dehydrate hexadecanol but are less active for esterification. Another consequence of fast dehydration rates of the alcohol on the bulk phosphides is the high yield of hexadecane observed on Ni_2P-CA, compared to Al_2O_3-supported Ni_2P. At present, we speculate that the reason of these differences is due to the fact that esterification is strongly dependent on steric hindrance, because the two bulky molecules, hexadecanol and palmitic acid, have to coincide on at least one acid site. Dehydration, in contrast, is a monomolecular reaction. Similar conclusions have been reached for transesterification and ether production [41,42]. Alumina would offer sites that both, hexadecanol and palmitic acid can access simultaneously, whereas the sites on bulk phosphides may favor monomolecular reactions. Alternatively, the type of acidity may lead to the observed differences, alumina is typically a material with high Lewis acidity, whereas the acid sites in the phosphide phase might originate from residual OH (Brønsted acid sites) groups. The details of this are currently under investigation.

4. Conclusions

The hydreoxygenation (HDO) performance of Ni_2P and MoP materials was explored (using palmitic acid as a model compound for bio-mass derived oils) in function of the identity of the transition metal, the presence of Al_2O_3 as a support and the synthesis procedure. For the synthesis of highly active bulk Ni_2P, citric acid was added during the synthesis, which led to a material with small crystal size, high specific surface, and a carbon structure acting as support for the phosphide phase. The concentration of metal sites, as determined by CO

adsorption increased as follows Ni_2P-CA ($0.23\ \mu mol\ g^{-1}$) < Ni_2P/Al_2O_3-LT ($0.29\ \mu mol\ g^{-1}$) < Ni_2P/Al_2O_3-TPR ($0.61\ \mu mol\ g^{-1}$) < MoP/Al_2O_3-TPR ($6.4\ \mu mol\ g^{-1}$) < MoP ($10\ \mu mol\ g^{-1}$). The TOFs of the HDO of palmitic acid increased in the order: MoP/Al_2O_3-TPR < MoP < Ni_2P-CA < Ni_2P/Al_2O_3-TPR < Ni_2P/Al_2O_3-LT (the TOFs of the Ni_2P catalysts were very similar). Hence, Ni_2P is intrinsically more active than MoP. The activity per gram of catalysts is determined by the interplay between this intrinsic activity and the concentration of metal sites accessible to the reactant giving the specific activity trend: MoP/Al_2O_3-TPR (high temperature synthesis) < Ni_2P-CA (citric acid in the synthesis) < Ni_2P/Al_2O_3-LT (low temperature synthesis) < Ni_2P/Al_2O_3-TPR < MoP.

Unsupported Ni_2P and MoP favored hydrodeoxygenation ($C_{15}H_{31}COOH \rightarrow C_{15}H_{31}CHO \rightarrow C_{16}H_{33}OH \rightarrow C_{16}H_{34}$) over decarbonylation ($C_{15}H_{31}COOH \rightarrow C_{15}H_{31}CHO \rightarrow C_{15}H_{32}$), and decarboxylation ($C_{15}H_{31}COOH \rightarrow C_{15}H_{32}$). Esterification ($C_{15}H_{31}COOH + C_{16}H_{33}OH \rightarrow C_{15}H_{31}COOC_{16}H_{33}$) does not significantly occur on unsupported phosphides. The presence of Al_2O_3 as a support significantly increased the rates of esterification due to its high concentration of acid sites. Interestingly, supporting Ni_2P on Al_2O_3 increased its selectivity towards decarbonylation and decarboxylation. As a result pentadecane was the favored product on Ni_2P/Al_2O_3, whereas C16 products dominate on MoP/Al_2O_3. For Ni_2P/Al_2O_3, a relative low-temperature method led to smaller phosphide particle size than more typical methods at high temperature. However, the catalyst with larger particle sizes was more active than the one with smaller particle size due to agglomeration of phosphide particles in the latter, which decreased its effective active surface. The activation energy for HDO is higher on Ni_2P than on MoP (112–120 kJ mol^{-1}, and 56–84 kJ mol^{-1}, respectively). This work demonstrates that MoP- and Ni_2P-based catalysts are active and stable in HDO applications. Further, the performance of the catalysts can be selectively tuned by varying the transition metal and adding a support.

Acknowledgements

The authors would like to thank Prof. Roel Prins for the critical discussion of the results. We also thank Dr. Stefano Cimino and Dr. Luciana Lisi for the scientific support. We are also grateful to Dr. Marianne Hanzlik for TEM measurements and to Dipl.-Ing. Xaver Hecht for technical support. G.M. thanks the DAAD for providing an international exchange grant (grant number A/13/71108).

Appendix A. Supplementary data

Supplementary data associated with this article can be found, in the online version, at http://dx.doi.org/10.1016/j.apcatb.2015.06.042

References

[1] E. Furimsky, Appl. Catal. A Gen. 199 (2000) 147–190.
[2] S.T. Oyama, Catal. Today 15 (1992) 179–200.
[3] B. Diaz, S.J. Sawhill, D.H. Bale, R. Main, D.C. Phillips, S. Korlann, R. Self, M.E. Bussell, Catal. Today 86 (2003) 191–209.
[4] Y. Liu, R. Sotelo-Boyás, K. Murata, T. Minowa, K. Sakanishi, Energy Fuels 25 (2011) 4675–4685.
[5] K. Murata, Y. Liu, M. Inaba, I. Takahara, Energy Fuels 24 (2010) 2404–2409.
[6] R. Sotelo-boy, Y. Liu, T. Minowa, Ind. Eng. Chem. Res. 50 (2011) 2791–2799.
[7] S.T. Oyama, T. Gott, H. Zhao, Y.-K. Lee, Catal. Today 143 (2009) 94–107.
[8] R. Prins, M.E. Bussell, Catal. Lett. 142 (2012) 1413–1436.
[9] A. Rodriguez, J. Kim, J.C. Hanson, S.J. Sawhill, M.E. Bussell, J. Phys. Chem. B. 107 (2003) 6276–6285.
[10] S. Sawhill, K. Layman, D. Vanwyk, M. Engelhard, C. Wang, M. Bussell, J. Catal. 231 (2005) 300–313.
[11] P. Liu, A. Rodriguez, J. Am. Chem. Soc. 127 (2005) 14871–14878.
[12] V.M.L. Whiffen, K.J. Smith, S.K. Straus, Appl. Catal. A Gen. 419–420 (2012) 111–125.
[13] V.M.L. Whiffen, K.J. Smith, Energy Fuels 24 (2010) 4728–4737.
[14] H.Y. Zhao, D. Li, P. Bui, S.T. Oyama, Appl. Catal. A Gen. 391 (2011) 305–310.
[15] K. Li, R. Wang, J. Chen, Energy Fuels 25 (2011) 854–863.
[16] B. Peng, Y. Yao, C. Zhao, J.A. Lercher, Angew. Chem. Int. Ed. Engl. 51 (2012) 2072–2075.
[17] J. Chen, H. Shi, L. Li, K. Li, Appl. Catal. B Environ. 144 (2014) 870–884.
[18] R. Wang, K.J. Smith, Appl. Catal. A Gen. 380 (2010) 149–164.
[19] V.M.L. Whiffen, K.J. Smith, Top. Catal. 55 (2012) 981–990.
[20] A. Montesinos-Castellanos, T.A. Zepeda, B. Pawelec, J.L.G. Fierro, J.A. de los Reyes, Chem. Mater. 19 (2007) 5627–5636.
[21] N. Rinaldi, Usman, T. Al-Dalama, Y. Okamoto, Appl. Catal. A Gen. 360 (2009) 130–136.
[22] C. Yu, J. Hu, W. Zhou, Q. Fan, J. Energy Chem. 23 (2014) 235–243.
[23] R. Cheng, Y. Shu, L. Li, J. Sun, X. Wang, T. Zhang, Thermochim. Acta 450 (2006) 42–46.
[24] P. Liu, A. Rodriguez, T. Asakura, J. Gómez, K. Nakamura, J. Phys. Chem. B 109 (2005) 4575–4583.
[25] P. Liu, J.A. Rodriguez, Y. Takahashi, K. Nakamura, J. Catal. 262 (2009) 294–303.
[26] P. Liu, A. Rodriguez, J. Am. Chem. Soc. 127 (2005) 14871–14878.
[27] S.T. Oyama, Y. Lee, J. Phys. Chem. B 109 (2005) 2109–2119.
[28] Y. Lee, S. Oyama, J. Catal. 239 (2006) 376–389.
[29] J.-S. Moon, E.-G. Kim, Y.-K. Lee, J. Catal. 311 (2014) 144–152.
[30] X. Yang, Z.H. He, X.J. Zhou, S.H. Xu, K.T. Leung, Appl. Surf. Sci. 252 (2006) 3647–3657.
[31] S. Yanagisawa, T. Tsuneda, K. Hirao, Y. Matsuzaki, J. Mol. Struct. Theochem. 716 (2005) 45–60.
[32] J. Lu, S. Behtash, A. Heyden, J. Phys. Chem. C. 116 (2012) 14328–14341.
[33] D. Mei, A.M. Karim, Y. Wang, ACS Catal. 2 (2012) 468–478.
[34] F. Delbecq, F. Vigné, J. Phys. Chem. B 109 (2005) 10797–10806.
[35] J.H. Sinfelt, Ad. Catal. 23 (1973) 91–119.
[36] A.F. Guillermet, M. Korling, Phys. Rev. 48 (1993) 11685–11691.
[37] Y. Liu, E. Lotero, J. Goodwinjr, J. Catal. 242 (2006) 278–286.
[38] B. Peng, C. Zhao, S. Kasakov, S. Foraita, J.A. Lercher, Chem. Eur. J. 19 (2013) 4732–4741.
[39] B. Peng, X. Yuan, C. Zhao, J.A. Lercher, J. Am. Chem. Soc. 134 (2012) 9400–9405.
[40] H. Knözinger, Angew. Chem. Int. Ed. 7 (1968) 791–805.
[41] S. Yan, S.O. Salley, K.Y. Simon Ng, Appl. Catal. A Gen. 353 (2009) 203–212.
[42] W. Turek, J. Haber, A. Krowiak, Appl. Surf. Sci. 252 (2005) 823–827.